This article has been accepted for inclusion in a future issue of this journal. Content is final as presented, with the exception of pagination.

A Temperature-Compensated Gallium Nitride Micromechanical Resonator

Azadeh Ansari, *Student Member, IEEE*, and Mina Rais-Zadeh, *Senior Member, IEEE*

***Abstract*— A GaN bulk acoustic wave resonator is presented in this letter, showing fundamental thickness-mode resonance at 2.18 GHz, with a quality factor (Q) of 655 and a coupling coefficient ($k_t{}^2$) of 1%. The resonator is integrated with an AlGaN/GaN high electron mobility transistor (HEMT); the integrated resonator/HEMT structure is coated with a silicon dioxide (SiO_2) passivation layer. It is shown that a 400-nm-thick SiO_2 layer reduces the temperature coefficient of frequency (TCF) of the GaN-based resonator by >50%, while improving Q and $k_t{}^2$ of the fundamental thickness-mode resonance. The effect of SiO_2 passivation layer is studied on $k_t{}^2$, Q, and TCF of the device. Furthermore, the effects of temperature and input RF power on the resonator performance are characterized.**

***Index Terms*— GaN, MEMS resonator, TCF, Q.**

I. Introduction

AlGaN/GaN high electron mobility transistors (HEMTs), showing high breakdown voltage, high electron mobility and sheet density are promising candidates for high-power applications at RF, microwave, and mm-wave frequencies. The AlGaN/GaN integrated circuit technology can benefit from high-frequency and low-noise GaN oscillators, which can enable a monolithic all-GaN transceiver. In order to realize such oscillators, AlGaN/GaN HEMTs can be integrated with GaN micromechanical resonators as the frequency selecting components. The significantly higher Q of micromechanical resonators as compared to LC tanks results in improved phase noise of the oscillator circuit. In addition to noise performance, oscillators need to be stable in a wide temperature range ($e.g.$, from −40 °C to 85 °C). Similar to silicon and aluminum nitride (AlN), GaN exhibits a negative temperature coefficient of elasticity (TCE), which results in a negative TCF value. Temperature compensation techniques, although relatively mature in silicon [1] and AlN-based piezoelectric MEMS [2], have not been shown for GaN BAW resonators to date.

Our group has reported on GaN resonators with frequencies ranging from 10s of MHz to 3 GHz in [3] and [4]. Other groups have also reported on lower-frequency GaN BAW [5] and surface acoustic wave (SAW) resonators [6], and most noticeably on AlGaN/GaN resonant body transistors [7]. In [8], we demonstrated an 8.7 GHz resonator integrated with an on-chip AlGaN/GaN HEMT (Fig. 1). In this letter, the temperature induced frequency drift of the device is reduced by ∼50%, by utilizing a 400 nm-thick SiO_2 layer. The SiO_2 layer also serves as a passivation layer for the AlGaN/GaN HEMT integrated with the GaN resonator, deposited at the same fabrication step. The effect of SiO_2 passivation layer on the resonator performance is simulated and compared against measurement. We show that the deposition of 400 nm SiO_2 improves the coupling coefficient and Q of the fundamental thickness-mode resonance while reducing the TCF value.

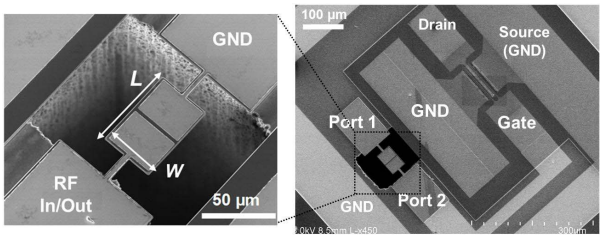

Device \ Dimensions (μm)	L	W	Tether Length	Tether Width
A	60	40	20	5
B	80	40	20	5

Fig. 1. (Top) Scanning electron microscope (SEM) images of a fabricated GaN BAW resonator integrated with an AlGaN/GaN HEMT, (bottom) summary of the device dimensions used in this letter.

II. Device Characterization

The resonator consists of 1.8 μm thick epitaxially grown GaN/AlGaN/AlN layer sandwiched between top and bottom gold electrodes, each 100 nm thick (Fig. 2(b)). The admittance (Y_{11}) of the uncompensated resonator (without the SiO_2 layer) is shown in Fig. 2(a) along with the mode shape at each thickness-mode harmonic simulated using COMSOL finite element modeling tool.

Mason's model is used to predict the impedance of the resonator [9]. This model translates each layer in the resonant stack to a T-network, based on the material's thickness and acoustic velocity defined as: $Z_{acs} = \rho \times \upsilon$, where ρ is the mass density and υ is the acoustic velocity in the material. C_C is the clamped capacitance given by $C_C = A/(\beta^S t)$, where A is the electrode area, t is the thickness of the piezoelectric layer, and β^S is the dielectric impermeability of the piezoelectric material at a constant strain. Φ denotes the coupling coefficient. Each series (Z_1) and shunt (Z_2) impedance in the T-network is given by:

$$Z_1 = -j \times Z_{acs} \times \tan\left(\frac{kt}{2}\right), \quad (1)$$

$$Z_2 = j \times Z_{acs} / \sin(kt), \quad (2)$$

where k is the wave number (Fig. 3(a)). Using this model, the predicted impedance plot is overlapped with the measured

Manuscript received July 15, 2014; revised August 13, 2014 and August 30, 2014; accepted September 11, 2014. This work was supported by the National Science Foundation under Award 1002036 and Award 1055308.1A. The review of this letter was arranged by Editor R. Quay.

The authors are with the Department of Electrical Engineering and Computer Science, University of Michigan, Ann Arbor, MI 48109 USA (e-mail: minar@umich.edu).

Color versions of one or more of the figures in this letter are available online at http://ieeexplore.ieee.org.

Digital Object Identifier 10.1109/LED.2014.2358577

0741-3106 © 2014 IEEE. Personal use is permitted, but republication/redistribution requires IEEE permission.
See http://www.ieee.org/publications_standards/publications/rights/index.html for more information.

This article has been accepted for inclusion in a future issue of this journal. Content is final as presented, with the exception of pagination.

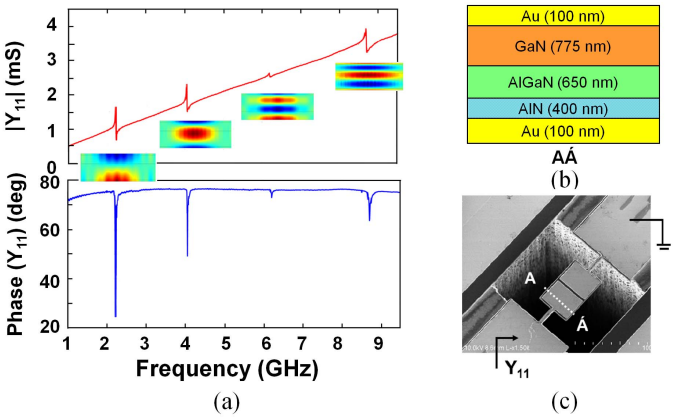

Fig. 2. (a) Simulated Y_{11} response of a GaN BAW resonator (Device A) and the 2D cross-section profile of the total displacement at each thickness-mode resonance harmonic. (b) Resonant stack showing the intended thickness of each layer. (c) One-port measurement setup: Port 2 is connected to GND.

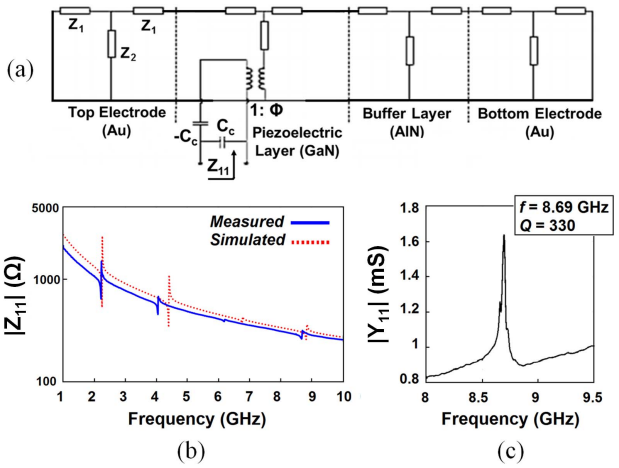

Fig. 3. (a) Mason's equivalent circuit model: each layer is translated to a T-network. (b) Z_{11} plot predicted by Mason's model (dotted red) and measured (blue) of Device A, predicting k_t^2 of 1.1% and 0.7% for the first and fourth-order thickness-mode respectively. (c) De-embedded Y_{11} of the fourth-order harmonic of Device A at room temperature and atmospheric pressure.

impedance plot (Fig. 3(b)). There is a good match between the measured and simulated results. The difference between the actual and intended thickness of each layer in the stack, the anchor design and the residual stress in the films are not taken into account in the Mason's model, which explains the discrepancy between the measured and simulated impedance plots. Fig. 3(c) shows the de-embedded Y_{11} of the fourth-order thickness-mode harmonic of the resonator. This mode exhibits a mechanical Q of 330 at 8.7 GHz, marking the highest resonance frequency measured for GaN BAW resonators with a high $f \times Q$ value of 2.87×10^{12}.

III. Power Measurements

The power handling and nonlinearity of the resonator are characterized, showing similar results for the first and fourth-order thickness-mode resonances. Third-order input intercept point (IIP_3) values are extracted in Figs. 4(a, b), showing the highest reported IIP_3 values of ∼30 dBm for GaN-based bulk resonators [10]. The 1-dB power compression point (P_{1-dB}) occurs at input power level (P_{in}) of 16 dBm for both the

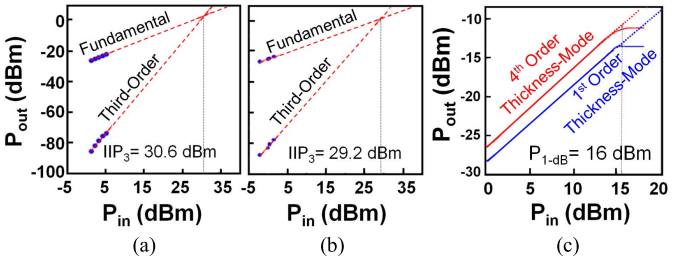

Fig. 4. Two-tone power measurements of the (a) first and (b) fourth-order thickness-mode harmonics of Device A. The IIP_3 value is extracted to be 30.6 dBm and 29.2 dBm, respectively, with a frequency separation of 5.1 kHz. (c) P_{1-dB} measurement showing P_{1-dB} of ∼16 dBm for both the first and the forth-order thickness-mode resonances. Different coupling coefficients could result in different IIP_3 values for the two modes.

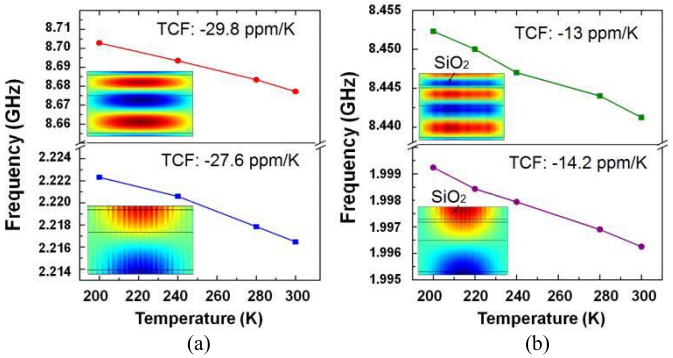

Fig. 5. Comparison of temperature trends for Device A (a) without and (b) with SiO_2 layer. It is worth mentioning that the level of temperature-compensation depends on the stress profile in the location of SiO_2 [14]. Lower TCF value achieved for the higher-order mode can be attributed to higher stress levels in SiO_2 for the higher-order resonance mode. (a) Non-passivated resonator (b) 400 nm SiO_2-passivated resonator.

first and fourth-order harmonics (Fig. 4(c)), suggesting that the power handling and device linearity are most likely limited by the anchor design and are independent of the operation mode.

IV. Temperature Effects

Effect of temperature on the resonator performance is studied in Fig. 5(a). The TCF of the resonator is measured to be ∼−30 ppm/K. The measured TCF in this letter is expected to be higher than the TCF reported for GaN BAW resonators in [3] due to the thicker AlN/AlGaN layer in the stack ($TCF_{AlN} \sim -25$ ppm/K [2], $TCF_{GaN} \sim -18$ ppm/K [3]), and also the presence of thick gold metal electrodes (10% of the entire stack) with a TCE of ∼−200 ppm/K [11]. Furthermore, the property of materials in this specific stack (*e.g.*, different level of doping for unintentionally doped GaN) could affect the resonator TCF. This level of temperature stability is unsuitable for any frequency reference application. Optimized doping and utilizing materials with positive TCE in the stack can reduce TCF values to enable temperature-stable oscillators.

To reduce the resonator TCF, a 400 nm thick SiO_2 layer is deposited on the resonator stack (Fig. 5). The SiO_2 layer also acts as the surface passivation layer for the AlGaN/GaN HEMTs, improving voltage break-down, frequency-dependent current leakage, and surface trappings [12]. Hence, by using this simple temperature-compensation approach, no additional step is added to the standard GaN MMIC process [13].

This article has been accepted for inclusion in a future issue of this journal. Content is final as presented, with the exception of pagination.

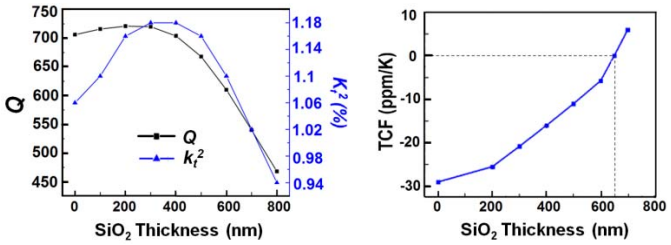

(a) (b)

Fig. 6. Simulation results, showing the effect of SiO_2 thickness on the fundamental thickness-mode response of Device B; (a) Q and k_t^2 using the Mason's model, taking into account only the acoustic impedance mismatch between the stack materials. (b) TCF vs. SiO_2 thickness, assuming TCE of $+160$ ppm/K for SiO_2 and -60 ppm/K for the GaN-based stack.

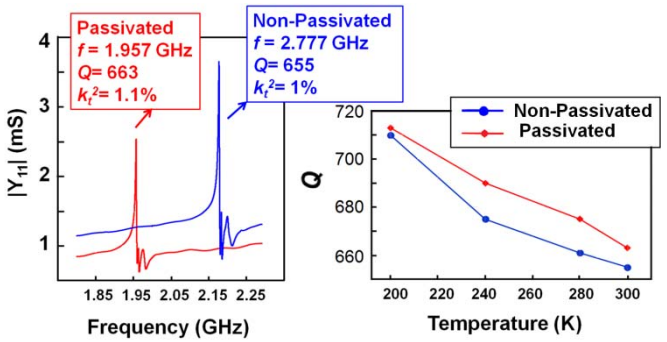

(a) (b)

Fig. 7. (a) Measured Y_{11} of the fundamental thickness-mode resonance of Device B, comparing the passivated and non-passivated resonance responses. Both Q and k_t^2 improve with 400 nm SiO_2 passivation. (b) Measured Q of Device B vs. temperature, showing a reduction of only 7% from 200 to 300 K.

The thickness of the SiO_2 is chosen to optimize the Q and k_t^2 of the resonator. The effect of SiO_2 thickness on k_t^2 and Q of the fundamental thickness-mode resonance of Device B is simulated using the Mason's model (Fig. 6(a)). The improvement in the simulated k_t^2 and Q with deposition of $\sim$400 nm of SiO_2 can be attributed to the improved distribution of acoustic standing wave energy within the stack. Fig. 6(b) studies the effect of SiO_2 thickness on the TCF of the fundamental thickness-mode resonance, showing that 650 nm thick SiO_2 can fully compensate the resonator TCF.

Fig. 7(a) shows the measured admittance response of the fundamental thickness-mode resonance of device B, indicating that deposition of 400 nm SiO_2 improves the Q from 655 to 663 and k_t^2 from 1 to 1.1% agreeing reasonably well with the Mason's model prediction in Fig. 6(a). It must be noted that the effect of stress in thin films is not captured by the Mason's model. Particularly, additional improvement in the measured device performance is expected as a result of stress cancellation with the deposition of SiO_2 layer on the released GaN/AlN stack. Table I summarizes the measured performance metrics of the fundamental thickness-mode resonance of Device B, verifying that depositing 400 nm of SiO_2 reduces TCF by $\sim$50%, improves Q and k_t^2, as predicted by simulations in Fig. 6. It is also worth mentioning that the small temperature dependence of the Q for the fundamental mode (Fig. 7(b)) suggests that the resonator loss is not limited by the phonon-phonon mechanism and an optimized design can improve the $f \times Q$ value from 1.4×10^{12} to the phonon-phonon Akheiser limit of $\sim10^{13}$ [15].

TABLE I

SUMMARY OF MEASURED PERFORMANCE METRICS FOR DEVICE B

Device B	*TCF* (ppm/K)	*Temp* (K)	Q	f_s (GHz)	f_p (GHz)	k_t^2 (%)
Non-passivated	-29	300	655	2.1772	2.1861	1
400 nm-SiO_2 passivated	-15	300	663	1.9576	1.9663	1.1

V. CONCLUSION

A thickness-mode GaN BAW resonator, integrated with an AlGaN/GaN HEMT is demonstrated in this letter. It is shown that a 400 nm thick SiO_2 surface passivation layer, used to improve the small signal and DC performance of the integrated AlGaN/GaN HEMT [12], can also reduce the TCF value of the GaN BAW resonator from ~ -30 ppm/K to ~ -13 ppm/K, while improving the k_t^2 and Q of the fundamental thickness resonance of the device. This letter is the first realization of a temperature-compensated GaN resonator with a blanket SiO_2 deposition and no additional fabrication steps. Further optimization of the location and thickness of the SiO_2 layer is needed to reach near zero TCF required for resonators used in timing references.

REFERENCES

[1] R. Melamud *et al.*, "Temperature-compensated high-stability silicon resonators," *Appl. Phys. Lett.*, vol. 90, no. 24, pp. 244107-1–244107-3, Jun. 2007.

[2] C.-M. Lin *et al.*, "Temperature-compensated aluminum nitride Lamb wave resonators," *IEEE Trans. Ultrason., Ferroelectr., Freq. Control*, vol. 57, no. 3, pp. 524–532, Mar. 2010.

[3] V. J. Gokhale, J. Roberts, and M. Rais-Zadeh, "High performance bulk mode gallium nitride resonators and filters," in *Proc. 16th Int. Trans. Conf. Solid-State Sens., Actuators Microsyst. Conf. (TRANSDUCERS)*, Beijing, China, Jun. 2011, pp. 926–929.

[4] A. Ansari *et al.*, "Gallium nitride-on-silicon micromechanical overtone resonators and filters," in *Proc. IEEE Int. Electron Device Meeting Conf.*, Washington, DC, USA, Dec. 2011, pp. 20.3.1–20.3.4.

[5] L. C. Popa and D. Weinstein, "L-band Lamb mode resonators in gallium nitride MMIC technology," in *Proc. Int. Freq. Control Symp.*, Taipei, Taiwan, May 2014, pp. 1–4.

[6] A. Shankar *et al.*, "Characterization of irradiated and temperature-compensated gallium nitride surface acoustic wave resonators," *Proc. SPIE*, vol. 9113, pp. 91130B-1–91130B-6, Jun. 2014.

[7] M. Faucher *et al.*, "Amplified piezoelectric transduction of nanoscale motion in gallium nitride electromechanical resonators," *Appl. Phys. Lett.*, vol. 94, no. 23, pp. 233506-1–233506-3, Jun. 2009.

[8] A. Ansari and M. Rais-Zadeh, "An 8.7 GHz GaN micromechanical resonator with an integrated AlGaN/GaN HEMT," in *Proc. Hilton Head Workshop*, Jun. 2014, pp. 295–296.

[9] W. P. Mason, *Electromechanical Transducers and Wave Filters*. New York, NY, USA: Van Nostrand, 1948.

[10] M. Rais-Zadeh *et al.*, "Gallium nitride as an electromechanical material," *IEEE/ASME J. Microelectromech. Syst.*, to be published

[11] Y. Chang and L. Himmel, "Temperature dependence of the elastic constants of Cu, Ag, and Au above room temperature," *J. Appl. Phys.*, vol. 37, no. 9, pp. 3567–3572, Aug. 1966.

[12] B. M. Green *et al.*, "The effect of surface passivation on the microwave characteristics of undoped AlGaN/GaN HEMTs," *IEEE Electron Device Lett.*, vol. 21, no. 6, pp. 268–279, Jun. 2000.

[13] M.-W. Ha *et al.*, "Silicon dioxide passivation of AlGaN/GaN HEMTs for high breakdown voltage," in *Proc. Int. Symp. Power Semicond. Devices ICs*, Jun. 2006, pp. 1–5.

[14] V. Thakar *et al.*, "Piezoelectrically transduced temperature-compensated flexural-mode silicon resonators," *J. Microelectromech. Syst.*, vol. 22, no. 3, pp. 815–823, Jun. 2013.

[15] V. J. Gokhale and M. Rais-Zadeh, "Phonon-electron interactions in piezoelectric semiconductor bulk acoustic wave resonators," *Nature Sci. Rep.*, vol. 4, Jul. 2014, Art. ID 5617.